Structural Aspects of Isozyme Selectivity in the Binding of Inhibitors to Carbonic Anhydrases II and IV

Chu-Young Kim,[†] Douglas A. Whittington,[†] Jeanne S. Chang,[†] John Liao,[‡] Jesse A. May,[‡] and David W. Christianson*,[†]

Roy and Diana Vagelos Laboratories, Department of Chemistry, University of Pennsylvania, Philadelphia, Pennsylvania 19104-6323, and Alcon Research, Ltd., 6201 South Freeway, Fort Worth, Texas 76134-2099

Carbonic anhydrase inhibitors are effective in lowering intraocular pressure, the primary indication of glaucoma. Human carbonic anhydrase II, and possibly carbonic anhydrase IV (CAII and CAIV, respectively), help regulate fluid secretion into the anterior chamber of the eye. Because inhibitors currently formulated as drugs to treat glaucoma were designed to target CAII, an understanding of the structural basis of CAII–CAIV discrimination by inhibitors would be useful for probing the role of each isozyme in the etiology of the disease. Here, we report the X-ray crystal structures of three novel thieno[3,2-*e*]-1,2-thiazine-6-sulfonamides complexed with CAII and the computationally predicted structures of the same compounds complexed with CAIV. All three compounds bind with similar affinity to CAII, but they bind with up to 100-fold lower affinities to CAIV. Comparisons of experimentally determined structures of CAII–inhibitor complexes and computationally predicted structures of CAIV–inhibitor complexes allow us to rationalize these affinity trends and outline molecular features that may contribute to high-affinity inhibitor binding to CAIV. This study demonstrates how experimental structure determination methods and computational structure prediction methods can be used together to answer questions that cannot be answered by either method alone.

Introduction

All mammals express one or more of the carbonic anhydrase (CA) isozymes, each of which catalyzes the conversion of carbon dioxide and water to bicarbonate and a proton.[1,2] Human carbonic anhydrase II (CAII), one of the most efficient isozymes with $k_{cat}/K_M = 1.5 \times 10^8$ M^{-1} s^{-1}, is found in the kidney, brain, pancreas, gastric mucosa, skeletal muscle, retina, and the lens.[3] Inhibitors of CA are successfully used to treat the main symptom of glaucoma, elevated intraocular pressure, which is responsible for retinal degeneration and blindness.[4–6] The inhibition of ocular CA decreases sodium and aqueous humor secretion, thereby lowering intraocular pressure. CAI, CAII, and CAIV are expressed in the human eye; CAII, and possibly CAIV, appears to play a greater role in regulating intraocular pressure.[7,8] Inhibitors of the CAs that are currently prescribed for glaucoma therapy, such as Diamox (acetazolamide),[9,10] Trusopt (dorzolamide),[11] and Azopt (brinzolamide),[12–15] are mainly used or designed to target CAII. CAII inhibitors typically exhibit lower affinity toward CAIV; for example, brinzolamide binds to CAII and CAIV with K_d values of 3.2 and 45.3 nM, respectively.[12–15] Therefore, the development of isozyme-specific CA inhibitors may ultimately benefit the treatment of glaucoma patients insofar as one particular isozyme might be predominantly responsible.

The X-ray crystal structure of human CAII was first reported by Liljas and colleagues,[16] and the structures of human and murine CAIVs were reported by Stams and colleagues.[17,18] Human CAII and CAIV are structurally and kinetically[2,19] quite similar despite the fact that CAII is a cytosolic protein and CAIV is a membrane-associated protein. The sequence identity between CAII and CAIV is 33%, and these isozymes share the same overall 10-stranded β-sheet fold. The active site of each isozyme contains a single zinc ion, which is coordinated by three histidine residues (His-94, His-96, and His-119) and a hydroxide ion at the bottom of a 15 Å deep hydrophobic cleft. Catalytically required residues Thr-199, Glu-106, and His-64 are conserved in CAII and CAIV. His-64 has been identified as the "proton shuttle" that transfers a proton from zinc-bound water to bulk solvent.[20] Two ordered water molecules between His-64 and Zn–OH$_2$ form a hydrogen bond network across which proton transfer is achieved by Grotthuss diffusion.[2,21]
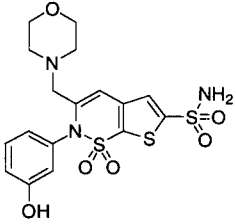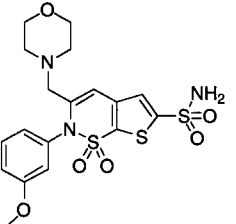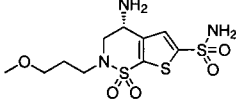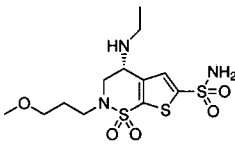
Two distinct His-64 conformations have been observed in CAII and CAIV crystal structures. His-64 can adopt the "in" conformation (with the imidazole ring directed toward zinc) or the "out" conformation (with the imidazole ring directed away from zinc). The X-ray crystal structure of native human CAII at pH 8.5 shows that His-64 predominantly adopts the in conformation,[21] whereas the crystal structure at pH 5.7 (at which His-64 is protonated) shows that His-64 adopts the out conformation.[22] In human CAIV, His-64 occupies the out conformation at pH 5.1, consistent with the behavior of His-64 in CAII.[17] However, in murine CAIV,[18] His-64 occupies the out conformation even at pH 7, which contrasts with the pH-dependent conformational behavior of this residue in the human isozymes. Importantly, the conformational change of His-64 to the out conformation is proposed to enhance inhibitor affinity in certain CAII–inhibitor complexes.[23]

* To whom correspondence should be addressed. Tel: (215)898-5714. Fax: (215)573-2201. E-mail: chris@xtal.chem.upenn.edu.
† University of Pennsylvania.
‡ Alcon Research, Ltd.

Table 1. CA Inhibitors

AL-6619[a]	AL-6629[a]	AL-8520[b]	AL-4862 (Brinzolamide)[c]
2*H*-Thieno[3,2-*e*]-1,2-thiazine-6-sulfonamide, 2-(3-hydroxyphenyl)-3-(4-morpholinylmethyl)-, 1,1-dioxide	2*H*-Thieno[3,2-*e*]-1,2-thiazine-6-sulfonamide, 2-(3-methoxyphenyl)-3-(4-morpholinylmethyl)-, 1,1-dioxide	2*H*-Thieno[3,2-*e*]-1,2-thiazine-6-sulfonamide, 4-amino-3,4-dihydro-2-(3-methoxypropyl)-, 1,1-dioxide, (R)	2*H*-Thieno[3,2-*e*]-1,2-thiazine-6-sulfonamide, 4-(ethylamino)-3,4-dihydro-2-(3-methoxypropyl)-, 1,1-dioxide, (R)

	CAII	CAIV		CAII	CAIV		CAII	CAIV		CAII	CAIV
IC_{50}	1.15 nM	4.25 nM		1.27 nM	7.41 nM		1.28 nM	128 nM		3.2 nM	45.3 nM

[a] Ref 24. [b] May, J. Unpublished results. [c] Ref 18.

The most notable structural difference between CAII and CAIV is found in the Lys-124–Glu-138 segment (CAIV numbering). In CAIV, this segment forms an ordered loop that extends away from the active site cavity (this loop is ordered in only one of the two molecules in the asymmetric unit[17]); in CAII, the corresponding segment is an α-helix.[21] Additionally, Pro-202 and Phe-131 lie at the mouth of the active site cleft in CAII. These residues are replaced with the smaller side chains of Thr-202 and Val-131 in CAIV. Consequently, the active site cleft of CAIV is less constricted than that of CAII. Differences in the structure and stability of the mouth of the active site of each isozyme may possibly be exploited in the design of isozyme-specific inhibitors.

As the first step toward the rational design of isozyme-specific CA inhibitors, we have determined the X-ray crystal structures of three structurally related sulfonamide inhibitors complexed with human CAII (Table 1).[12–15,24] Strikingly, these inhibitors bind to CAII with similar affinity, but they bind to CAIV with up to 100-fold weaker affinity. Such affinity differences are likely due to pendant "tail" groups that interact differently with the mouth of each isozyme active site. Because of difficulties in preparing inhibitor complexes with human CAIV, we have predicted the structures of human CAIV–inhibitor complexes using computational methods. The CAs are ideal candidates for such structural and computational studies of inhibitor binding because numerous crystal structures of enzyme–inhibitor complexes determined to date show that few conformational changes of enzyme residues accompany inhibitor binding. Thus, CAII and CAIV are essentially static ligand receptor molecules, which simplifies structural and computational analysis.

Results

X-ray Crystal Structures of CAII–Inhibitor Complexes. Electron density maps of the CAII complexes with AL-6619, AL-6629, and AL-8520 reveal inhibitor binding conformations clearly and unambiguously (Figure 1). The binding modes of the *exo*-sulfonamide and
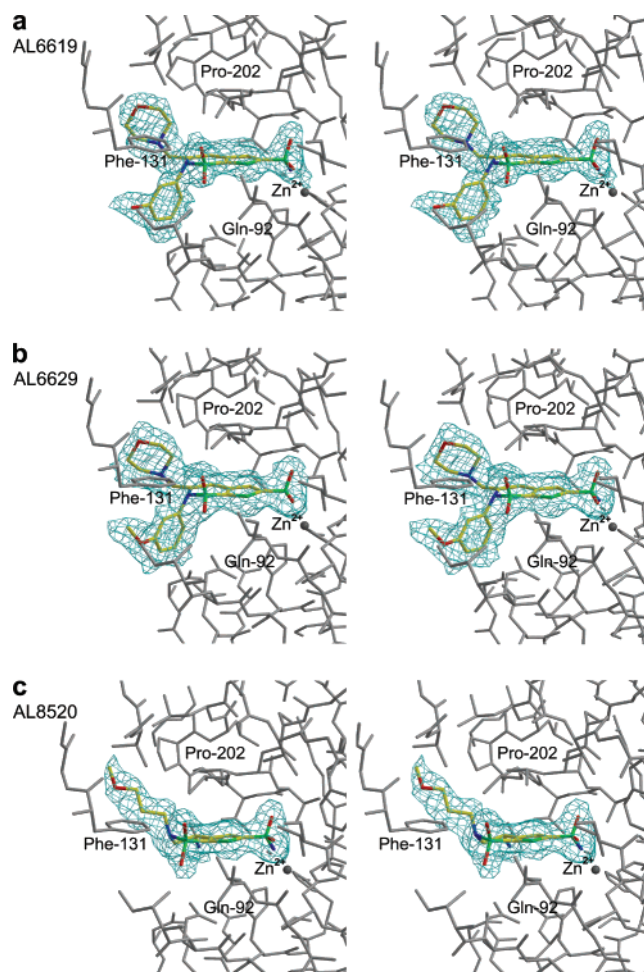

Figure 1. Difference electron density maps calculated with Fourier coefficients $|F_o| - |F_c|$ and phases derived from the final model less the inhibitor and active site solvent molecules. Maps are contoured at 2.2σ: (a) CAII–AL-6619 complex; (b) CAII–AL-6629 complex; (c) CAII–AL-8520 complex. Selected active site residues are indicated.

the adjacent bicyclic ring structure are identical for each inhibitor: the ionized sulfonamide NH group coordinates to zinc and donates a hydrogen bond to the

hydroxyl side chain of Thr-199, and a sulfonamide S=
O group accepts a hydrogen bond from the backbone NH
group of Thr-199. The *endo*-sulfonamide of each inhibi-
tor likewise makes identical interactions: one S=O
group accepts a hydrogen bond from Gln-92, and the
other S=O group accepts a weak C−H hydrogen bond
from Phe-131. These interactions are characteristic for
the binding of thienothiazine-6-sulfonamides to CAII.[18,25]

Notably, His-64 shifts to the out conformation in each
enzyme−inhibitor complex, even though it is not steri-
cally forced to do so. At pH 8.0, the in conformer is
expected to predominate. Possibly, the conformational
change of His-64 to the out conformation may contribute
to enhanced enzyme−inhibitor affinity due to the dis-
placement of a bound water molecule.[23]

The interactions of the pendant tail groups are similar
for AL-6619 and AL-6629: the morpholino group as-
sociates with the hydrophobic patch defined by Phe-131,
Val-135, and Pro-202, and the meta-substituted phenyl
group makes van der Waals contact with Asn-67, Ile-
91, and Phe-131. AL-6619 and AL-6629 differ by only
the methylation of the meta hydroxyl group, so it is not
too surprising that the overall binding conformations
of these inhibitors are nearly identical. The aliphatic
ether tail of AL-8520 associates with the hydrophobic
patch defined by Phe-131, Val-135, and Pro-202. Note
that this same region of the hydrophobic cleft is occupied
by the morpholino group in the binding of AL-6619 and
AL-6629. The primary amine donates a hydrogen bond
to Thr-200.

It is interesting to note that the configuration of the
endo-sulfonamide nitrogen differs for aromatic substit-
uents (AL-6619, AL6629) and aliphatic substituents
(AL-8520). Accordingly, the *endo*-sulfonamide substit-
uents occupy different locations in the enzyme active
site: the meta-substituted phenyl groups of AL-6619
and AL-6629 occupy the Ile-91 canyon, whereas the
aliphatic ether tail of AL-8520 occupies the Val-135
canyon (Figure 2). Apparently, specific interactions in
the Ile-91 canyon (e.g., the orientation of the enzyme−
inhibitor aromatic−aromatic interaction and/or other
weakly polar interactions with the inhibitor aromatic
ring) contribute to binding differences between inhibi-
tors bearing aromatic or aliphatic substituents on the
endo-sulfonamide nitrogen. Moreover, the binding of the
morpholino groups of AL-6619 and AL-6629 in the Val-
135 canyon disfavors an *endo*-sulfonamide configuration
that would simultaneously place its aromatic substitu-
ent in this narrow canyon (Figure 2).

Because the structure of AL-8520 differs from that
of AL-4862 (brinzolamide) by just a single *N*-ethyl
substituent (Table 1), it is useful to summarize the
binding mode of the CAII−AL-4862 complex.[18] The *exo*-
sulfonamide and *endo*-sulfonamide groups of AL-4862
make interactions with the enzyme active site identical
to those of AL-6619, AL-6629, and AL-8520. The ali-
phatic ether tail contacts Phe-131, Val-135, and Pro-
202, and the ethylamine NH group donates a hydrogen
bond to Thr-200. Importantly, the ethylamine group
sterically forces His-64 to adopt the out conformation.

**Computationally Predicted Structures of CAIV−
Inhibitor Complexes.** The structures of AL-6619, AL-
6629, AL-8520, and AL-4862 complexed with CAIV were
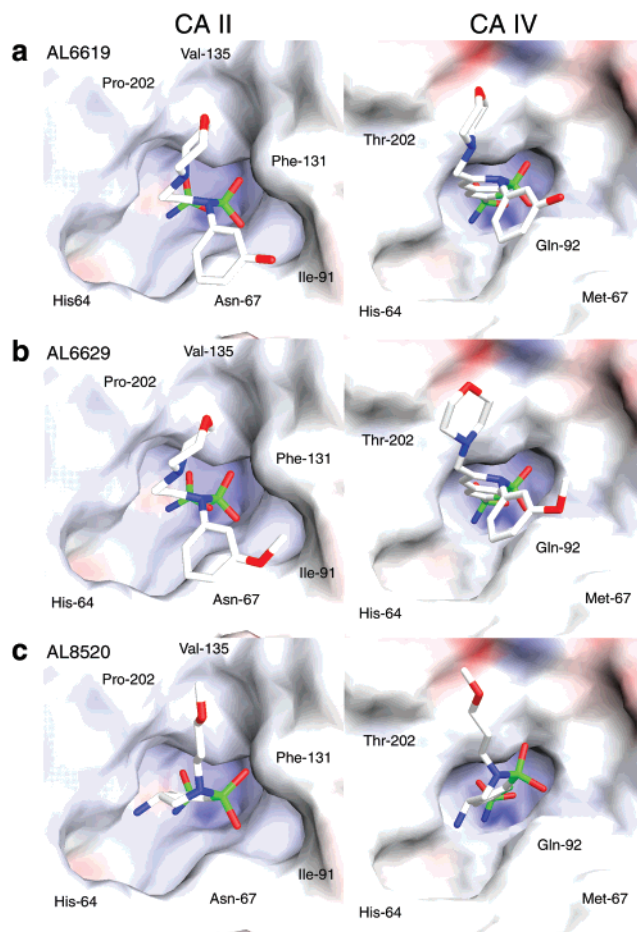predicted by three-dimensional structural alignment;

Figure 2. Left: X-ray crystal structures of CAII−inhibitor
complexes. Right: predicted structures of CAIV−inhibitor
complexes. (a) CAII−AL-6619 and CAIV−AL-6619 complexes;
(b) CAII−AL-6629 and CAIV−AL-6629 complexes; (c) CAII−
AL-8520 and CAIV−AL-8520 complexes. Selected active site
residues are indicated. Electrostatic surface potentials were
generated by GRASP.[31]

i.e., each CAII−inhibitor crystal structure was super-
imposed onto CAIV and then the energy of the respec-
tive CAIV−inhibitor complex was minimized as sum-
marized in the Experimental Section. Given the observed
conformational mobility of His-64 in CAII and given the
apparent impact of this mobility on inhibitor binding
affinity, two different CAIV conformers, CAIV−His-64$_{in}$
and CAIV−His-64$_{out}$, were used in energy minimiza-
tions. Both His-64 conformers yielded similar predicted
structures of CAIV−inhibitor complexes for all inhibi-
tors except for AL-4862 (Figure 3). Just as the ethyl-
amino group of AL-4862 sterically requires the confor-
mational change of His-64 to accommodate binding to
CAII, it is reasonable to expect the same requirement
to accommodate binding to CAIV.

The predicted binding modes of the *exo*-sulfonamide
and the adjacent bicyclic ring structures are identical
for each inhibitor and resemble those observed in the
corresponding, experimentally determined CAII−inhibi-
tor complexes: the ionized sulfonamide NH group
coordinates to zinc and donates a hydrogen bond to the
hydroxyl side chain of Thr-199, and a sulfonamide S=
O group accepts a hydrogen bond from the backbone NH
group of Thr-199. An *endo*-sulfonamide oxygen atom of
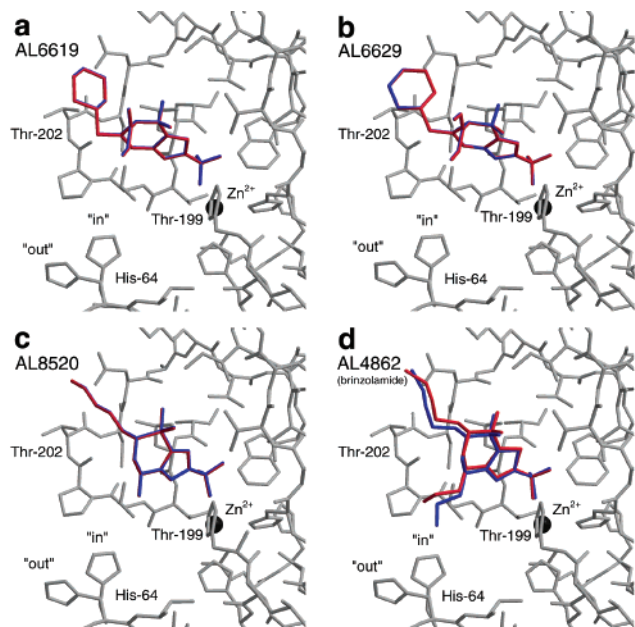each inhibitor accepts a hydrogen bond from Gln-92 in

Figure 3. Superpositions of modeled structures of CAIV−His-64_{in}−inhibitor complexes (red) and modeled structures of CAIV−His-64_{out}−inhibitor complexes (blue). (a) CAIV−AL-6619 complex; (b) CAIV−AL-6629 complex; (c) CAIV−AL-8520 complex; (d) CAII−AL-4862 complex. Selected active site residues are indicated.

the predicted models of their complexes with CAIV. The pendant tail groups of AL-6619 and AL-6629 make identical interactions in the CAIV active site: the meta-substituted phenyl ring of each inhibitor contacts Gln-92, and the morpholino group is positioned adjacent to the wall of the active site lined by Thr-202, Asp-204, and Lys-206. The aliphatic ether tail of AL-8520 is positioned similarly to the morpholino groups of AL-6619 and AL-6629, i.e., adjacent to the surface lined by residues Thr-202 and Asp-204; the ether oxygen atom makes no hydrogen bond interactions. Likewise, the primary amine group of AL-8520 makes no hydrogen bond interactions, although its proximity to the side chain of Thr-200 and the presence of water suggest at least a potential for hydrogen bond interactions. Finally, the aliphatic ether tail of AL-4862 is similarly positioned to that of AL-8520, and the ethylamine group lies adjacent to the enzyme surface lined by Trp-5 and Thr-200; the ethylamine NH group makes no hydrogen bond interactions.

Discussion

The main objective of this study is the determination of the structural basis of isozyme selectivity for inhibitor binding to CAII and CAIV. Crystal structures of CAII−inhibitor complexes are compared with predicted structures of CAIV−inhibitor complexes in Figures 2 and 4. In CAII, two "canyons" at the mouth of the hydrophobic cleft accommodate inhibitor pendant tail groups: the Val-135 canyon is flanked by Pro-202 and Phe-131, and the Ile-91 canyon is flanked by Phe-131 and Asn-67. The morpholino (AL-6619 and AL-6629) and aliphatic ether (AL-8520) tail groups occupy the Val-135 canyon, while the meta-substituted phenyl rings (AL-6619 and AL-6629) occupy the Ile-91 canyon. Because AL-6619, AL-6629, and AL-8520 exhibit similar IC_{50} values (Table 1), the contribution of the tail groups to the overall binding affinity must be similar for all three cases.

All four X-ray crystal structures of the CAII−inhibitor complexes reveal that His-64 adopts the out conformation, although AL-4862 is the only inhibitor in this series to sterically require the conformational change of His-64 for binding. Because AL-6619, AL-6629, and AL-8520 do not sterically force His-64 to move from the native in conformation to the observed out conformation, His-64 movement may instead arise from other subtle conformational and solvation changes in the protein tertiary structure triggered by inhibitor binding.

CAIV docking simulations similarly show that the binding of AL-4862 is sensitive to the His-64 conformation, whereas the binding of AL-6619, AL-6629, and AL-8520 is independent of the His-64 conformation. AL-4862 is anchored to the enzyme by the *exo*-sulfonamide−zinc interaction and by a hydrogen bond between the *endo*-sulfonamide and the Gln-92. The absence of strong anchoring interactions for the inhibitor aliphatic ether tail and the conformational mobility of the 130's segment in the CAIV active site that potentially destabilizes inhibitor binding likely result in the 14-fold lower affinity of AL-4862 toward CAIV as compared with CAII (Table 1).

As compared to that of CAII, the hydrophobic cleft of CAIV has a less constricted contour due to the Lys-124−Glu-138 loop that extends away from the active site. CAIV contains no canyon corresponding to the Ile-91 canyon of CAII, and the canyon corresponding to the Val-135 canyon of CAII is much broader (Figure 2). This broad canyon in CAIV accommodates the morpholino (AL-6619 and AL-6629) and aliphatic ether (AL-8520
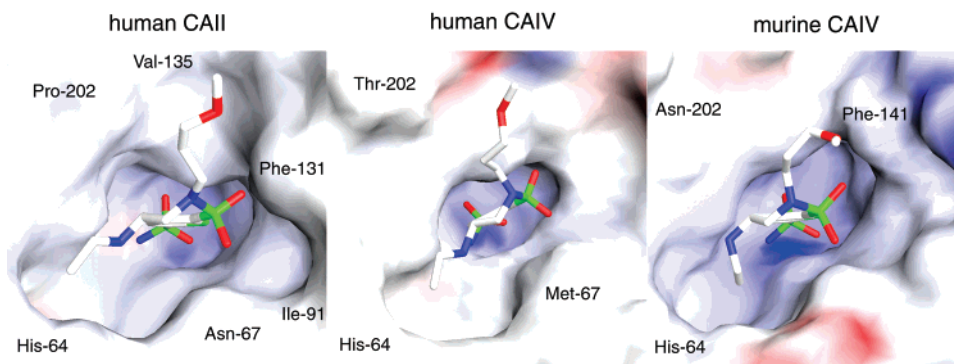

Figure 4. From left to right: human CAII−AL-4862 complex (X-ray crystal structure);[18] human CAIV−AL-4862 complex (predicted structure); murine CAIV−AL-4862 complex (X-ray crystal structure).[18] Electrostatic surface potentials were generated by GRASP.[31]

Table 2. Data Collection and Refinement Statistics for CAII−Inhibitor Complexes

inhibitor	AL-6619	AL-6629	AL-8520
no. of measd reflctns	119 808	54 642	55 023
no. of unique reflctns	19 173	16 912	15 945
max resolution (Å)	1.93	2.10	2.00
R_{merge}[a]	0.075	0.105	0.098
completeness of data (%)	93.6	99.1	92.6
no. of reflctns used in refinement ($>2\sigma$)	17 682	15 740	13 579
no. of reflctns in R_{free} test set	848	767	734
R_{cryst}[b]	0.223	0.155	0.158
R_{free}[c]	0.293	0.208	0.229
no. of nonhydrogen atoms[d]	2102	2090	2094
no. of solvent molecules included in refinement	107	179	176
rms dev from ideal bond lengths (Å)	0.011	0.009	0.009
rms dev from ideal bond angles (°)	1.6	1.7	1.6
rms dev from ideal dihedral angles (°)	25.3	25.1	24.8
rms dev from ideal improper angles (°)	1.5	1.3	1.6
RCSB accession code	1I91	1I8Z	1I90

[a] R_{merge} for replicate reflections, $R_{merge} = \sum |I_h - \langle I_h \rangle|/\sum \langle I_h \rangle$; I_h = intensity measured for reflection h, $\langle I_h \rangle$ = average intensity for reflection h calculated from replicate data. [b] Crystallographic R factor, $R_{cryst} = \sum ||F_o| - |F_c||/\sum |F_o|$; $|F_o|$ and $|F_c|$ are the observed and calculated structure factor amplitudes, respectively, for those reflections not included in the R_{free} test set. [c] Free R factor, $R_{free} = \sum ||F_o| - |F_c||/\sum |F_o|$ for only those reflections included in the R_{free} test set. [d] In asymmetric unit.

and AL-4862) tail groups of inhibitors. The relatively bulky morpholino and meta-substituted phenyl groups of AL-6619 and AL-6629 provide for more extensive contact surface area than the narrow aliphatic ether tail groups of AL-8520 or AL-4862 with the broad canyon in CAIV. This phenomenon may rationalize the CAIV−inhibitor affinity trends observed in Table 1, i.e., that nanomolar affinity toward CAIV is maintained by AL-6619 and AL-6629. We speculate that an inhibitor with a sufficiently bulky tail may bind preferentially to CAIV, since such a large tail group will not fit in the relatively constricted Val-135 canyon of CAII.

The binding of AL-4862 (brinzolamide) is of particular interest because it is currently formulated for glaucoma therapy as Azopt. The X-ray crystal structures of the human CAII−brinzolamide and the murine CAIV−brinzolamide complexes have been reported.[18] In Figure 4, we compare these experimentally determined structures with the computationally predicted structure of the human CAIV−brinzolamide complex. Note that the mouth of the cleft is markedly different in each of the three isozymes. Human CAII contains a three-turn α-helix (containing Phe-131) that divides the Ile-91 and Val-135 canyons. In human and murine CAIV, this polypeptide segment is either disordered or adopts an extended loop conformation, which results in a single, much broader canyon instead of two smaller canyons. Consequently, brinzolamide binds differently in each case. As with other inhibitors investigated in this study, the binding conformation of brinzolamide is highly complementary to the contour of the human CAII active site, whereas brinzolamide fits more "loosely" in the human CAIV and murine CAIV active sites (Figure 4). The lack of a narrow canyon corresponding to the Val-135 canyon of CAII appears to be responsible for the loss of inhibitor affinity to CAIV. Moreover, the conformational mobility of this polypeptide segment in human and murine CAIVs may additionally compromise inhibitor binding affinity.

Conclusions

A combination of X-ray crystallographic and computational methods are used together to understand the structural basis of inhibitor affinity variations in binding to CAII and CAIV. Although three-dimensional structural alignment and energy minimization prove to be an effective tool in this study, we note that in more general applications special care must always be exercised to account for possible conformational changes of the protein receptor. In the case of CAII−inhibitor and CAIV−inhibitor complexes, the prediction problem is simplified because apart from the conformational mobility of His-64, these enzymes are essentially static receptors. Accordingly, comparisons of the experimentally determined structures of CAII−inhibitor complexes and computationally predicted structures of CAIV−inhibitor complexes reveal the molecular basis for inhibitor affinity variations between the two isozymes.

Experimental Section

CAII Crystallography. Human CAII was crystallized in 2.60−2.75 M ammonium sulfate and 50 mM Tris-sulfate (pH 8.0) at 4 °C using the hanging drop method. The protein solution contained 8−12 mg/mL CAII, 1 mM methyl mercuric acetate, and 50 mM Tris-sulfate (pH 8.0). Crystals appeared within 1 week and grew to full size in 2 weeks.

Prior to inhibitor soaking, CAII crystals were cross-linked by adding 5 μL of glutaraldehyde solution (0.8% glutaraldehyde (v/v), 4.0 M ammonium sulfate, and 50 mM Tris-sulfate (pH 8.0)) to the hanging drop and allowing it to equilibrate at 4 °C for 72 h. Each cross-linked crystal was transferred to a 10 μL drop containing a stabilization buffer of 3.5 M ammonium sulfate and 50 mM Tris-sulfate (pH 8.0). One microliter of inhibitor solution (10 mM inhibitor dissolved in dimethyl sulfoxide) was added to this drop and allowed to equilibrate at 4 °C for 1 week.

Crystals of the enzyme−inhibitor complexes were mounted in 0.7 mm glass capillaries. The X-ray diffraction data were collected at room temperature using an R-AXIS IIc image plate detector (Molecular Structure Corporation) with a Rigaku RU-200HB rotating anode generator (operating at 50 kV and 100 mA) supplying Cu Kα radiation focused with Yale double mirrors. The raw diffraction data were processed using the HKL suite of programs.[26] Crystals of enzyme−inhibitor complexes were isomorphous with those of native CAII, belonging to space group $P2_1$ with typical unit cell parameters $a = 42.7$ Å, $b = 41.4$ Å, $c = 72.9$ Å, and $\beta = 104.5°$. The 1.54 Å resolution structure of native human CAII retrieved from the Research Collaboratory for Structural Bioinformatics (RCSB accession code, 2CBA) was used as the starting coordinate set for the refinement of each enzyme−inhibitor complex structure.[21] Electron density maps, calculated with Fourier coefficients $2|F_o| - |F_c|$ and $|F_o| - |F_c|$, and phases derived from the in-progress atomic model were generated with X-PLOR.[27] The

inhibitor and solvent molecules in the active site were modeled in when the R factor dropped below 0.25; the graphics software O was used for map fitting and model building.[28] Refinement converged smoothly to final crystallographic R factors within the range of 0.165−0.198. Data refinement and collection statistics are recorded in Table 2. Coordinates of all enzyme−inhibitor complexes have been deposited in the RCSB with accession codes designated in Table 2.

CAIV Modeling. Three-dimensional structural alignment was utilized to predict the structure of each CAIV−inhibitor complex using the experimentally determined structure of the corresponding CAII−inhibitor complex as a starting point. The 2.8 Å resolution X-ray structure of the human CAIV−sulfate complex (RCSB accession code 1ZNC)[17] was used for structure alignment experiments. There are two molecules of CAIV in the asymmetric unit, designated A and B. The two chains have similar structural features (rms deviation = 0.2 Å) except in the Lys-124−Glu-138 region: in chain A, this segment is well-ordered and forms an extended loop while in chain B, this segment is disordered and thus absent from the final model. The atomic coordinates of chain A, less sulfate, Hg^{2+}, and water molecules were used for modeling experiments.

Inhibitor molecules were placed in the CAIV active site by overlaying the CAII−inhibitor structures onto the CAIV structure using 23 conserved residues that lined the active site cleft (rms deviation ∼ 0.9 Å). The energies of CAIV−inhibitor structures were then minimized as a function of atomic coordinate positions using the conjugate gradient energy minimization routine in the program CNS; standard protein topology and parameter files were employed.[29] Topology and parameter files for the inhibitors were constructed by using XPLO2D[30] and edited appropriately. To mimic the known primary binding interactions of the aromatic sulfonamides with CA, constraints on the *exo*-sulfonamide nitrogen−zinc bond and the *exo*-sulfonamide oxygen−Thr-199 backbone amide hydrogen bond were imposed during energy minimization. The remainder of each inhibitor molecule was free to seek the minimum energy location and conformation within the CAIV active site cleft.

References

(1) Hewett-Emmett, D.; Tashian, R. E. Functional diversity, conservation, and convergence in the evolution of the α-, β-, and γ-carbonic anhydrase gene families. *Mol. Phylogenet. Evol.* **1996**, *5*, 50−77.

(2) Silverman, D. N.; Lindskog, S. The catalytic mechanism of carbonic anhydrase: implications of a rate-limiting protolysis of water. *Acc. Chem. Res.* **1988**, *21*, 30−36.

(3) Maren, T. H. Carbonic anhydrase. Chemistry, physiology, and inhibition. *Physiol. Rev.* **1967**, *47*, 595−781.

(4) Friedenwald, J. S. The formation of the intraocular fluid *Am. J. Ophthalmol.* **1949**, *32*, 9−27.

(5) Kinsey, V. E. Comparative chemistry of aqueous humor in posterior and anterior chambers of rabbit eye. *Arch. Ophthalmol.* **1953**, *50*, 401−417.

(6) Maren, T. H. Carbonic anhydrase: general perspectives and advances in glaucoma research. *Drug Dev. Res.* **1987**, *10*, 255−276.

(7) Hageman, G. S.; Zhu, X. L.; Waheed, A.; Sly, W. S. Localization of carbonic anhydrase IV in a specific capillary bed of the human eye. *Proc. Natl. Acad. Sci. U.S.A.* **1991**, *88*, 2716−2720.

(8) Maren, T. H.; Wynns, G.; Wistrand, P. J. Chemical properties of carbonic anhydrase IV, the membrane-bound enzyme. *Mol. Pharmacol.* **1993**, *44*, 901−905.

(9) Becker, B. Decrease in intraocular pressure in man by a carbonic anhydrase inhibitor, Diamox. *Am. J. Ophthalmol.* **1954**, *37*, 13−15.

(10) Breinin, G. M.; Gortz, H. Carbonic Anhydrase Inhibitor Acetazolamide (Diamox). *Arch. Ophthalmol.* **1954**, *52*, 333−348.

(11) Lippa, E. A.; Carlson, L. E.; Ehinger, B.; Eriksson, L. O.; Finnstrom, K.; Holmin, C.; Nilsson, S. E.; Nyman, K.; Raitta, C.; Ringvold, A.; et al. Dose response and duration of action of dorzolamide, a topical carbonic anhydrase inhibitor. *Arch. Ophthalmol.* **1992**, *110*, 495−499.

(12) Camras, C. B.; The Brinzolamide Primary Therapy Study Group. A triple-masked, primary therapy study of the efficacy and safety of BID and TID-dosed Brinzolamide 1.0% compared to TID-dosed dorzolamide 2.0% and BID timolol 0.5%. *Invest. Ophthalmol. Visual Sci.* **1997**, *38*, S560.

(13) Dean, T. R.; May, J.; Chen, H. H.; Kyba, E.; McLaughlin, M.; DeSantis, L. Brinzolamide (AL-4862) suspension is a new topically active carbonic anhydrase inhibitor in the dutch-belted rabbit and cynomolgus monkey. *Invest. Ophthalmol. Visual Sci.* **1997**, *38*, S813.

(14) Shin, D. H.; The Brinzolamide Adjunctive Therapy Group. A triple-masked, placebo-controlled, adjunctive therapy study of the efficacy and safety of TID-dosed Brinzolamide 1.0% compared to the TID-dosed placebo when used adjunctively to timolol 0.5%. *Invest. Ophthalmol. Visual Sci.* **1997**, *38*, S559.

(15) Stewart, R.; The Brinzolamide Comfort Study Group. The ocular comfort of TID-dosed Brinzolamide 1.0% compared to TID-dosed dorzolamide 2.0% in patients with primary open-angle glaucoma or ocular hypertension. *Invest. Ophthalmol. Visual Sci.* **1997**, *38*, S559.

(16) Liljas, A.; Kannan, K. K.; Bergsten, P. C.; Waara, I.; Fridborg, K.; Strandberg, B.; Carlbom, U.; Jarup, L.; Lovgren, S.; Petef, M. Crystal structure of human carbonic anhydrase C. *Nature New Biol.* **1972**, *235*, 131−137.

(17) Stams, T.; Nair, S. K.; Okuyama, T.; Waheed, A.; Sly, W. S.; Christianson, D. W. Crystal structure of the secretory form of membrane-associated human carbonic anhydrase IV at 2.8 Å resolution. *Proc. Natl. Acad. Sci. U.S.A.* **1996**, *93*, 13589−13594.

(18) Stams, T.; Chen, Y.; Boriack-Sjodin, P. A.; Hurt, J. D.; Liao, J.; May, J. A.; Dean, T.; Laipis, P.; Silverman, D. N.; Christianson, D. W. Structures of murine carbonic anhydrase IV and human carbonic anhydrase II complexed with brinzolamide: molecular basis of isozyme-drug discrimination. *Protein Sci.* **1998**, *7*, 556−563.

(19) Baird, T. T., Jr.; Waheed, A.; Okuyama, T.; Sly, W. S.; Fierke, C. A. Catalysis and inhibition of human carbonic anhydrase IV. *Biochemistry* **1997**, *36*, 2669−2678.

(20) Tu, C.; Silverman, D. N.; Forsman, C.; Jonsson, B. H.; Lindskog, S. Role of histidine 64 in the catalytic mechanism of human carbonic anhydrase II studied with a site-specific mutant. *Biochemistry* **1989**, *28*, 7913−7918.

(21) Håkansson, K.; Carlsson, M.; Svensson, L. A.; Liljas, A. Structure of native and apo carbonic anhydrase II and structure of some of its anion-ligand complexes. *J. Mol. Biol.* **1992**, *227*, 1192−1204.

(22) Nair, S. K.; Christianson, D. W. Unexpected pH-dependent conformation of His-64, the proton shuttle of carbonic anhydrase II. *J. Am. Chem. Soc.* **1991**, *113*, 9455−9458.

(23) Smith, G. M.; Alexander, R. S.; Christianson, D. W.; McKeever, B. M.; Ponticello, G. S.; Springer, J. P.; Randall, W. C.; Baldwin, J. J.; Habecker, C. N. Positions of His-64 and a bound water in human carbonic anhydrase II upon binding three structurally related inhibitors. *Protein Sci.* **1994**, *3*, 118−125.

(24) Chen, H.-H.; Gross, S.; Liao, J.; McLaughlin, M.; Dean, T.; Sly, W. S.; May, J. A. 2*H*-Thieno[3,2-*e*]- and [2,3-*e*]-1,2-thiazine-6-sulfonamide 1,1-dioxides as ocular hypotensive agents: synthesis, carbonic anhydrase inhibition and evaluation in the rabbit. *Bioorg. Med. Chem.* **2000**, *8*, 957−975.

(25) Boriack-Sjodin, P. A.; Zeitlin, S.; Chen, H.-H.; Crenshaw, L.; Gross, S.; Dantanarayana, A.; Delgado, P.; May, J. A.; Dean, T.; Christianson, D. W. Structural analysis of inhibitor binding to human carbonic anhydrase II. *Protein Sci.* **1998**, *7*, 2483−2489.

(26) Otwinowski, Z.; Minor, W. Processing of X-ray diffraction data collected in oscillation mode. *Methods Enzymol.* **1997**, *276*, 307−326.

(27) Brünger, A. T.; Kuriyan, J.; Karplus, M. Crystallographic R factor refinement by molecular dynamics. *Science* **1987**, *235*, 458−460.

(28) Jones, T. A.; Zou, J. Y.; Cowan, S. W.; Kjeldgaard, M. Improved Methods for Building Protein Models in Electron Density Maps and the Location of Errors in These Models. *Acta Crystallogr.* **1991**, *A47*, 110−119.

(29) Brünger, A. T.; Adams, P. D.; Clore, G. M.; DeLano, W. L.; Gros, P.; Grosse-Kunstleve, R. W.; Jiang, J. S.; Kuszewski, J.; Nilges, M.; Pannu, N. S.; Read, R. J.; Rice, L. M.; Simonson, T.; Warren, G. L. Crystallography & NMR System: A New Software Suite for Macromolecular Structure Determination. *Acta Crystallogr.* **1998**, *D54*, 905−921.

(30) Kleywegt, G. J. Dictionaries for Heteros. *ESF/CCP4 Newsletter* **1995**, *31*, 45−50.

(31) Nicholls, A.; Sharp, K. A.; Honig, B. Protein folding and association: insights from the interfacial and thermodynamic properties of hydrocarbons. *Proteins: Struct., Funct., Genet.* **1991**, *11*, 281−296.